© Universiti Tun Hussein Onn Malaysia Publisher's Office

PAAT

http://publisher.uthm.edu.my/ojs/index.php/paat

e-ISSN : 2821-2924

Progress in Aerospace and Aviation Technology

Comparison of Flow Topology Between Major Groups of Airfoil with Vortex Shedding

Rizuan Miasin[1], Aslam Abdullah[1*], Mohd Fadhli Zulkafli[1]

[1]Department of Aeronautic Engineering, Faculty of Mechanical and Manufacturing Engineering, Universiti Tun Hussein Onn Malaysia, Parit Raja, Batu Pahat, 86400, MALAYSIA

*Corresponding Author

DOI: https://doi.org/10.30880/paat.2022.02.02.005
Received 15 November 2022; Accepted 19 December 2022; Available online 31 December 2022

Abstract: The effect of vortex behavior on airfoil aerodynamic performance has been widely debated for many years, and many research studies have been conducted to examine the relationship. This paper highlights the in-depth study of flow topological processes on major airfoil groups with vortex shedding. It considers various type of corresponding geometries including symmetrical, asymmetrical, thick, and thin airfoils in order to show the differences in flow topology. The study also emphasized the behavior of separation bubbles, vortex shedding and reattachment points. The use of a commercial CFD software for the study gave reliable results within an adequate length of time. The vortex shedding was successfully highlighted either physically or hypothetically. The separation bubble was relatively easier to be identified in all cases of airfoil of interest. The evolution of separation bubble captured by the topology in the case of Eppler 169 was the unique, and involved the break of reattachment point.

Keywords: Vortex shedding, airfoil, flow topology, separation bubble, CFD

1. Introduction

Over the years, extensive discussions of flow topology [1,2] have sparked motivation to study in more depth the process of vortex formation and the periodic behavior of reattachment profiles [3,4]. Despite clear methodology, the study of such flow topology has not yet covered most types of airfoils.

This study considered several types of airfoil that represent thick-thin and symmetrical-asymmetric airfoils. The computational fluid dynamics simulations that have been carried out involve the flow of air passing through this model. Attention was given mainly to separation bubbles and vortex shedding. The objective is to identify and comparatively study the flow topologies around symmetric-thick, asymmetric-thin, symmetric-thin, and asymmetric-thick airfoils. This simulation method could be validated against the analytical technique, which uses a special mathematical relationship. The results can be utilized in a variety of aviation applications as in the improvement of aerodynamic performance of airfoils with respect to vortex shedding, separation bubble and reattachment phenomena.

2. Methodology

We used a CFD software to analyze airfoils' flow and vortex shedding. There were four types of airfoil considered in the study; symmetrical, asymmetrical, thin and thick airfoils. These airfoils are categorized as either NACA or Eppler series shown in Fig. 1 to Fig. 4. Eppler 169 and Eppler 61 represent symmetric-thick, asymmetric-thin airfoils, respectively, while NACA 0008 and NACA 2411 indicate symmetric-thin, asymmetric-thick airfoils, respectively. The information on grid, domain, and boundary condition is given in Fig. 5.

*Corresponding author: aslam@uthm.edu.my

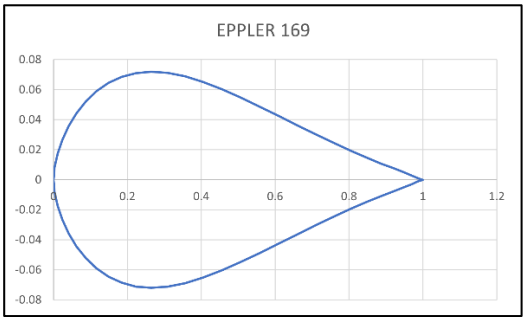

Fig. 1 - Eppler 169

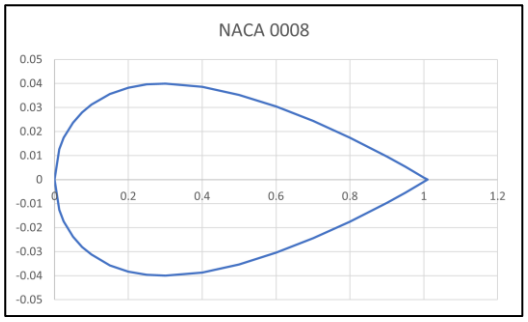

Fig. 2 - NACA 0008

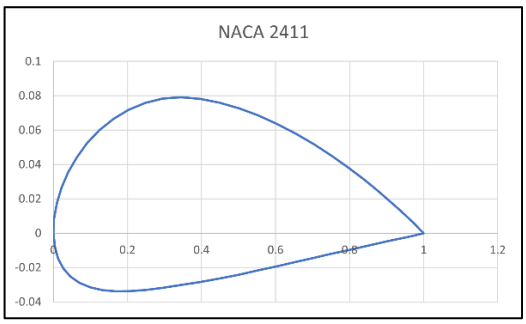

Fig. 3 - NACA 2411

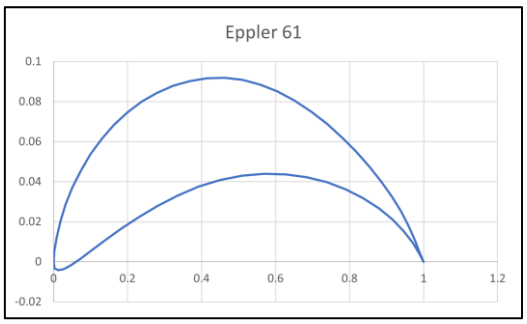

Fig. 4 - Eppler 61

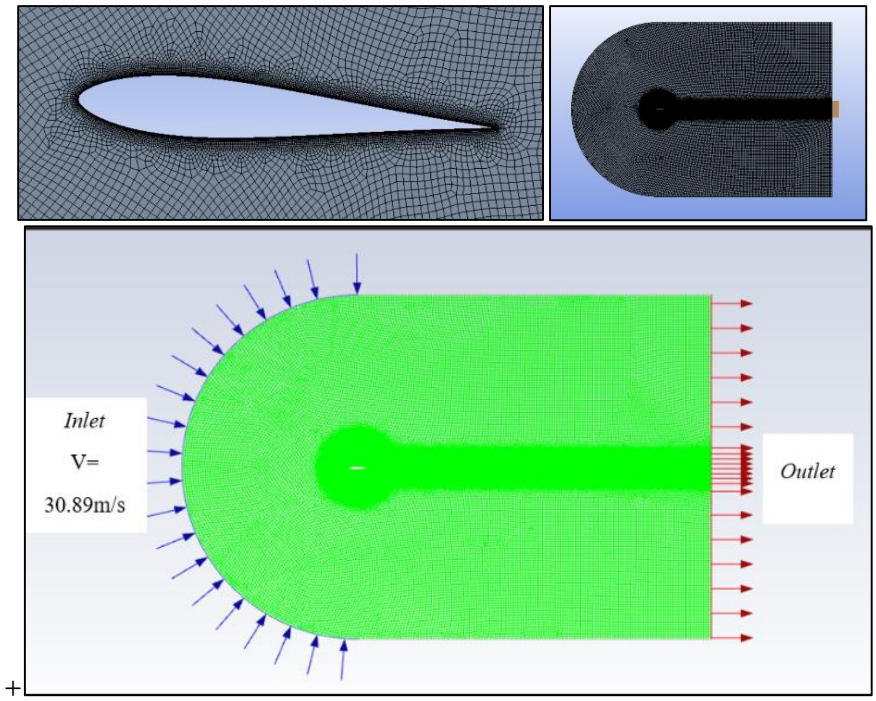

Fig. 5 - Grid, domain, and boundary condition

The parameter values used in the simulations are similar to those used in the previous study [5]. The flow model was set to laminar because it is suitable to observe flow topology and vortex shedding [5-10]. Topological overview of a flow was used in this study to determine the separation bubble profile as well as vortex shedding. The density was fixed and transient flow mode was set to get velocity curl profile over the airfoils with respect to time. The sample of airfoils' coordinates were obtained from an online database. The geometry scale of each airfoil was reduced from 1 m to 0.01 m to facilitate model design, and the angle of attack was set at 4º.

Density based solver was applied, and air velocity was set to be absolute. Laminar flow model was considered with no energy equation. The values for density and viscosity were kept constant, i.e. 1.225 kg/m^3 and 1.7894 x 10^{-5} kg/m-s, respectively. No-slip condition was assumed at the wall, and x-velocity magnitude was set to 30.89 m/s. The solution method was that of implicit Roe-FDS flux type, while the spatial discretization was that of least squares cell-based flow

which was that of second order upwind. The transient formulation was second order implicit. The report definition was added which included drag and lift coefficients. Standard solution initialization was implemented where the computation begins from the inlet. The output was automatically saved every 8 time steps. Contour of vorticity magnitude was plotted within the range of 5 s^{-1} to 3000 s^{-1}. Fixed time stepping method was used for the simulation, where time step size was 0.0015 with 600 number of time steps.

Studies on topological flows over major groups of airfoil such as those of symmetrical, asymmetrical, thick, and thin airfoils are important in the design of airfoils, rotor blades, propellers, and other applications of aeronautical engineering [11,12].

3. Result and Discussion

The results displayed in this section were calculated using a CFD software and further discussion is presented accordingly. The results were also checked and confirmed against the literature, in particular Hunt relationship [2], where fixed-point location and type were successfully validated.

$$\left(\Sigma \mathrm{E} + \frac{1}{2}\Sigma \mathrm{E}'\right) - \left(\Sigma \mathrm{H} + \frac{1}{2}\Sigma \mathrm{H}'\right) = 1 - n \tag{1}$$

where E is four-way elliptic, His four-way hyperbolic, E *'* is three-way elliptic, H *'* is three-way hyperbolic fixed points, and *n* is regional connectivity.

3.1 Eppler 61

At t_1 as in Fig. 6, it was found that no fixed-point movement occurred on the airfoil surface. The hyperbolic fixed point only appeared at the leading edge of the airfoil. In contrast, at t_2 as shown in Fig. 7, the hyperbolic fixed point H_1 at t_2 has indicated the starting point to the separation bubble. At t_3 and t_4 as in Fig. 8 and 9, there were also significant changes where the hyperbolic fixed point, H_1 and H_2 at t_3 on the trailing edge of the airfoil surface have collided with each other and caused the formation of a new hyperbolic fixed point H_1^* at t_4.

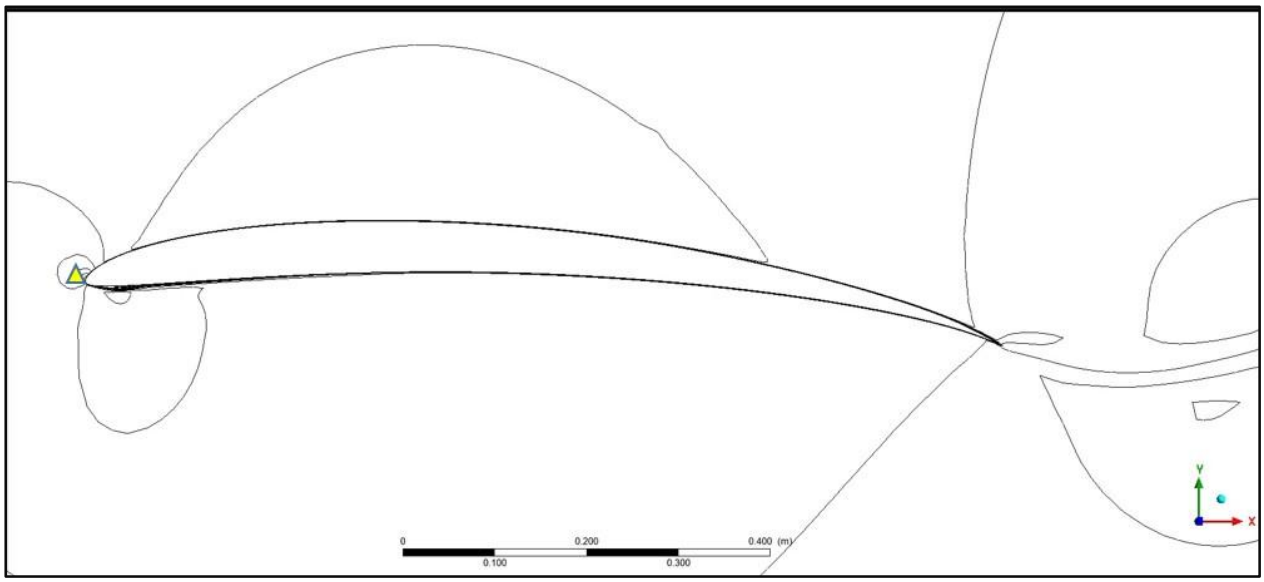

Fig. 6 - Flow topology around Eppler 61 at t_1 and α = 4°

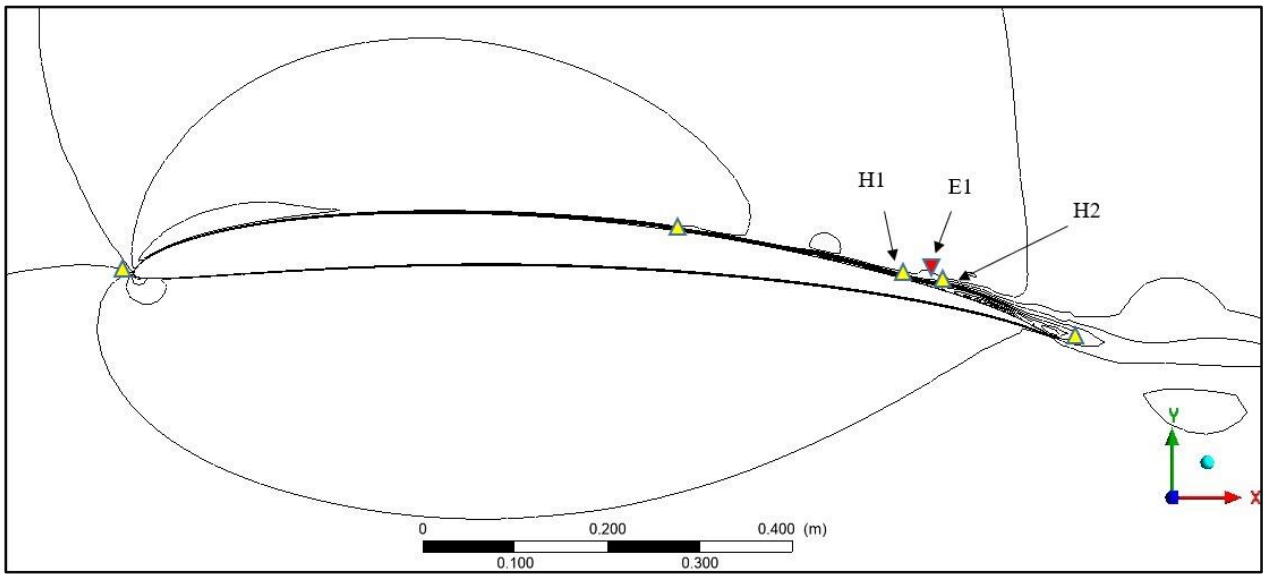

Fig. 7 - Flow topology around Eppler 61 at t_2 and $\alpha = 4°$

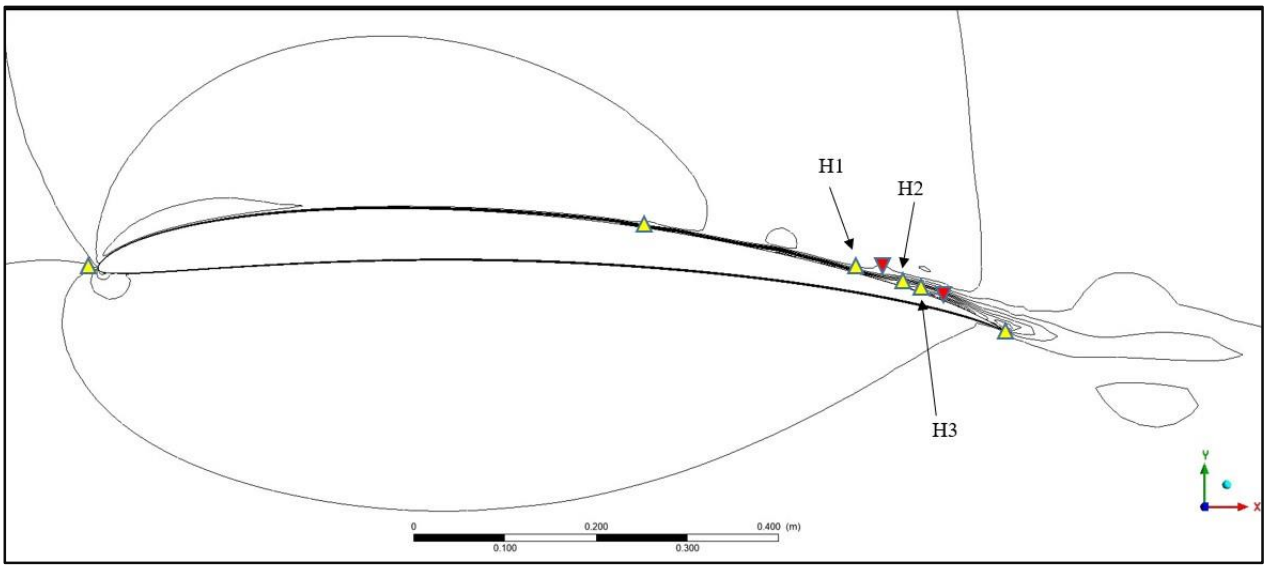

Fig. 8 - Flow topology around Eppler 61 at t_3 and $\alpha = 4°$

At t_4 and t_5 as in Fig. 9 and 10, there was not much significant change after a new hyperbolic fixed point H_1^* was formed. At t_6 as in Fig. 11, it could be expected that hyperbolic fixed points H_1^* and H_3 will collide, separate from the airfoil's surface, and create a new hyperbolic point of a shed vortex.

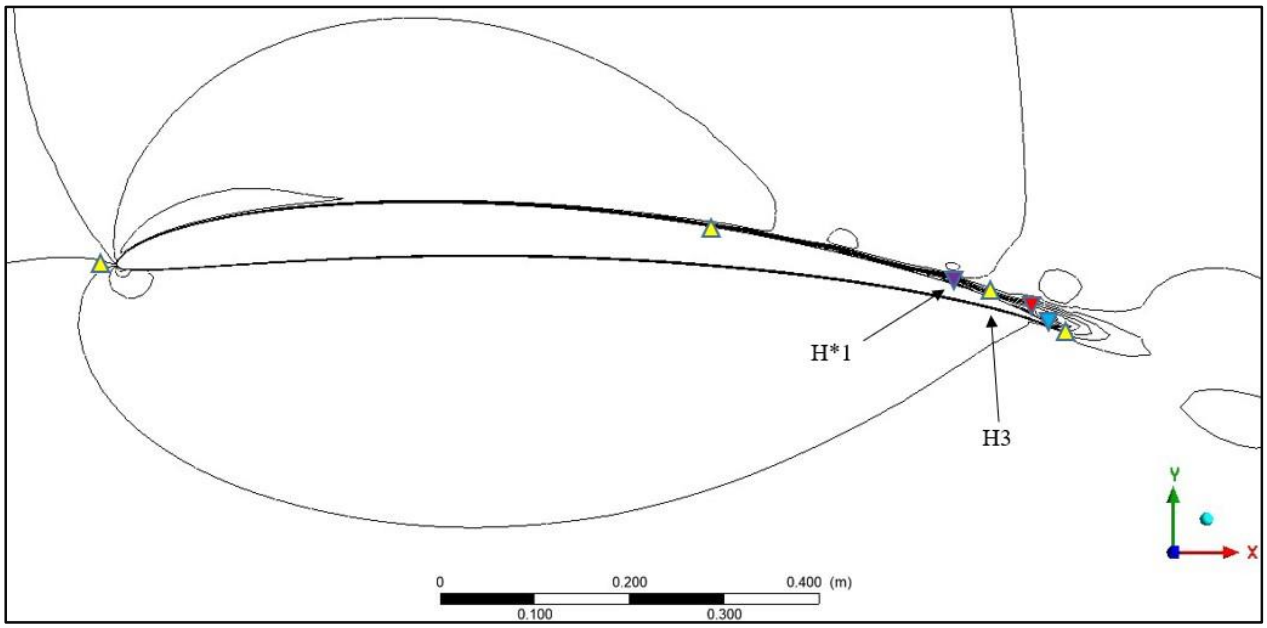

Fig. 9 - Flow topology around Eppler 61 at t_4 and $\alpha = 4^o$

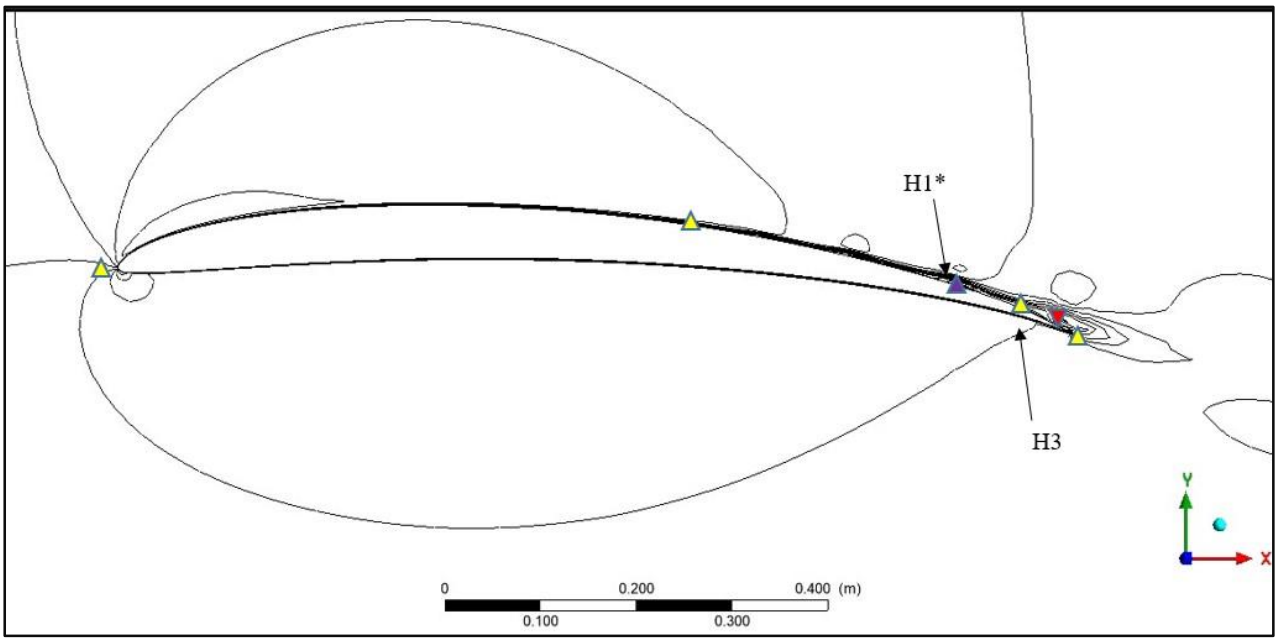

Fig. 10 - Flow topology around Eppler 61 at t_5 and $\alpha = 4^o$

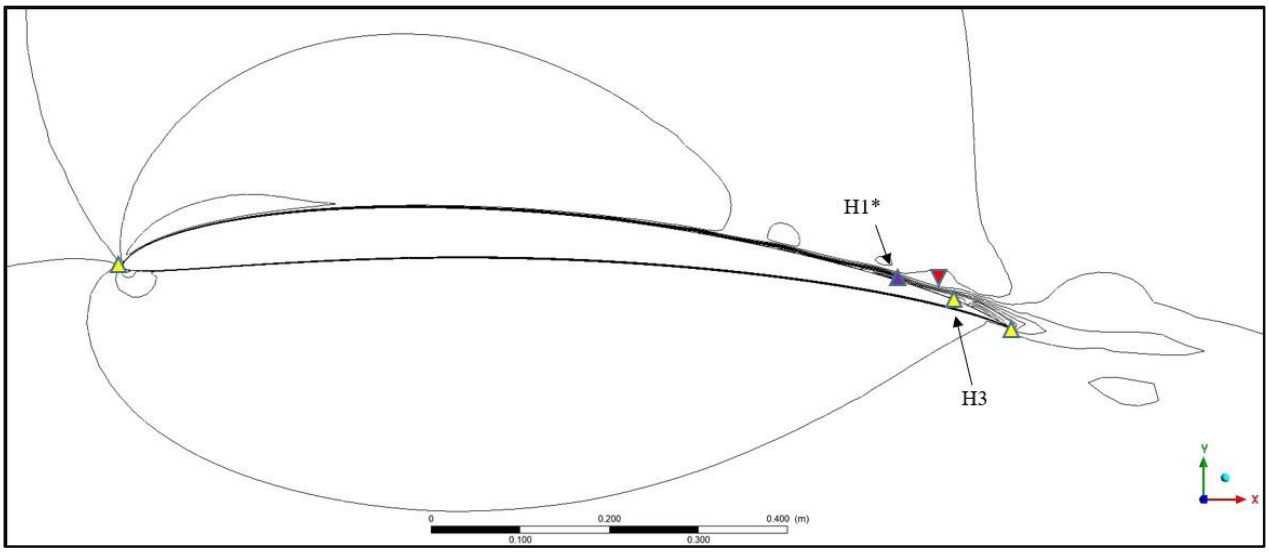

Fig. 11 - Flow topology around Eppler 61 at t_6 and $\alpha = 4^o$

3.2 NACA 2411

At t_1 as in Fig. 12, there was a beginning of flow topology change where the leading edge of the airfoil had a hyperbolic fixed point. However, at t_2 and t_3 as in Fig. 13 and 14, there were two hyperbolic fixed points, H_1 and H_2, which could be seen at the middle of the airfoil surface. There was a collision between hyperbolic H_3 and elliptic E_2 fixed points from t_2 to t_3 which in turn formed a reverse saddle node bifurcation pointing to the trailing edge of the airfoil.

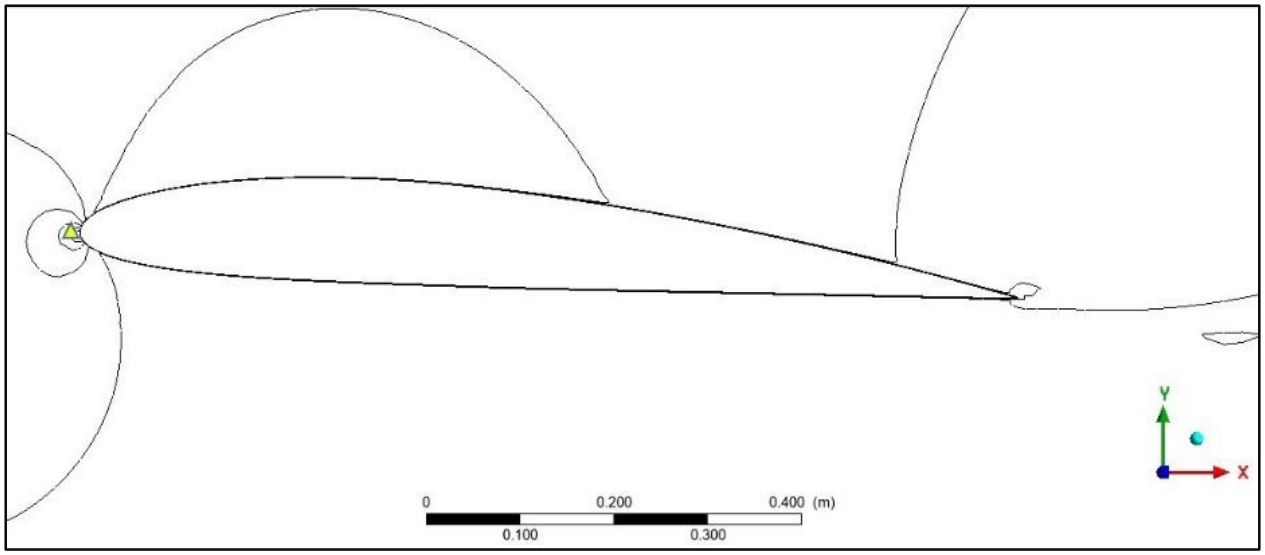

Fig. 12 - Flow topology around NACA 2411 at t_1 and $\alpha = 4^o$

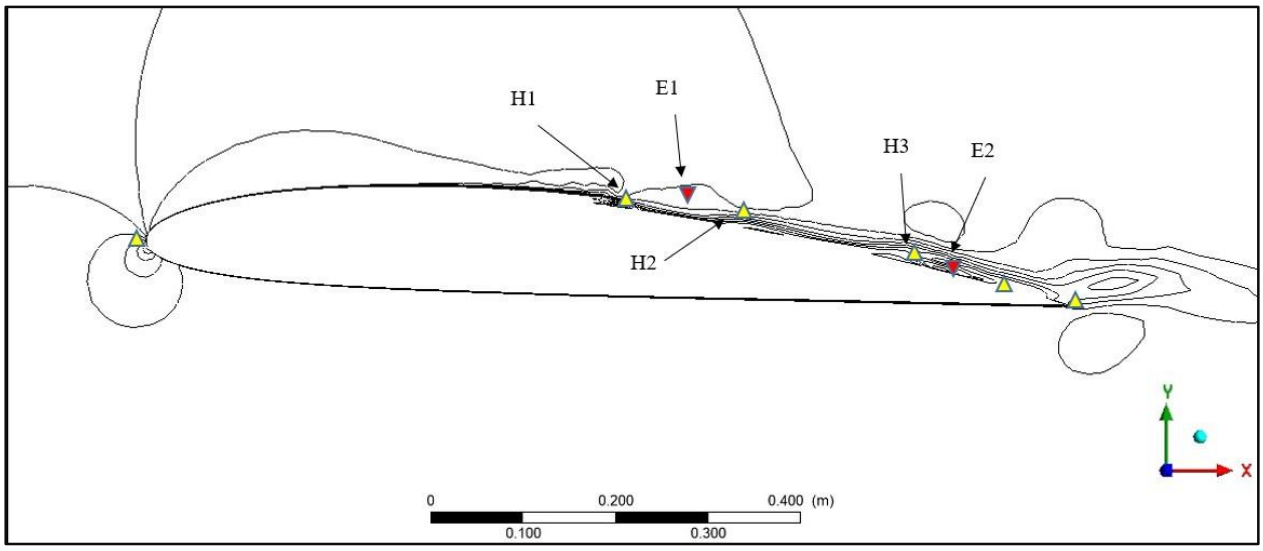

Fig. 13 - Flow topology around NACA 2411 at t_2 and $\alpha = 4^o$

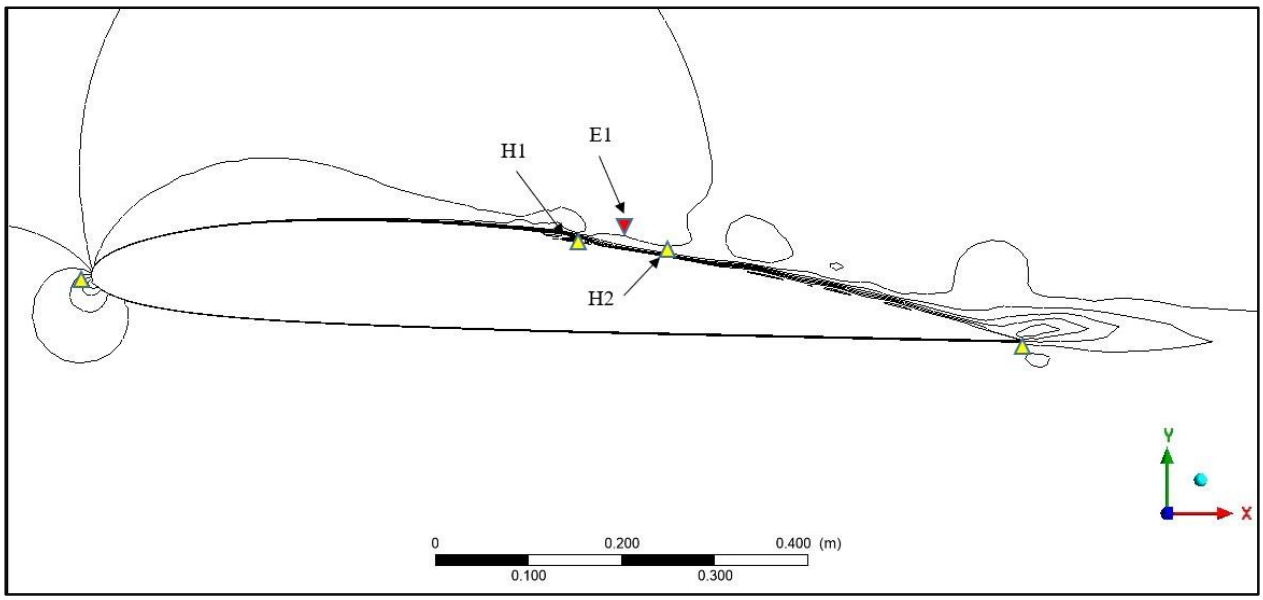

Fig. 14 - Flow topology around NACA 2411 at t_3 and $\alpha = 4^o$

At t_4 as in Fig. 15, it was observed that the arrangement of fixed points H_1 , H_2 and E_1 was similar to that at t_3 as in Fig. 14. There was a separation bubble on the surface near trailing edge. Meanwhile, at t_5 as in Fig. 16, there was a sign of collision in the middle of airfoil surface between the two hyperbolic fixed point, H_1 and H_2, under the elliptic fixed point, E_1. Consequently, the collision took place and created a new hyperbolic fixed point, H_1^* of a shed vortex at t_6 as shown in Fig. 17. It can be seen in Fig. 16 and Fig. 17 that near trailing edge, there was a topological flow pattern. However, no further process was captured.

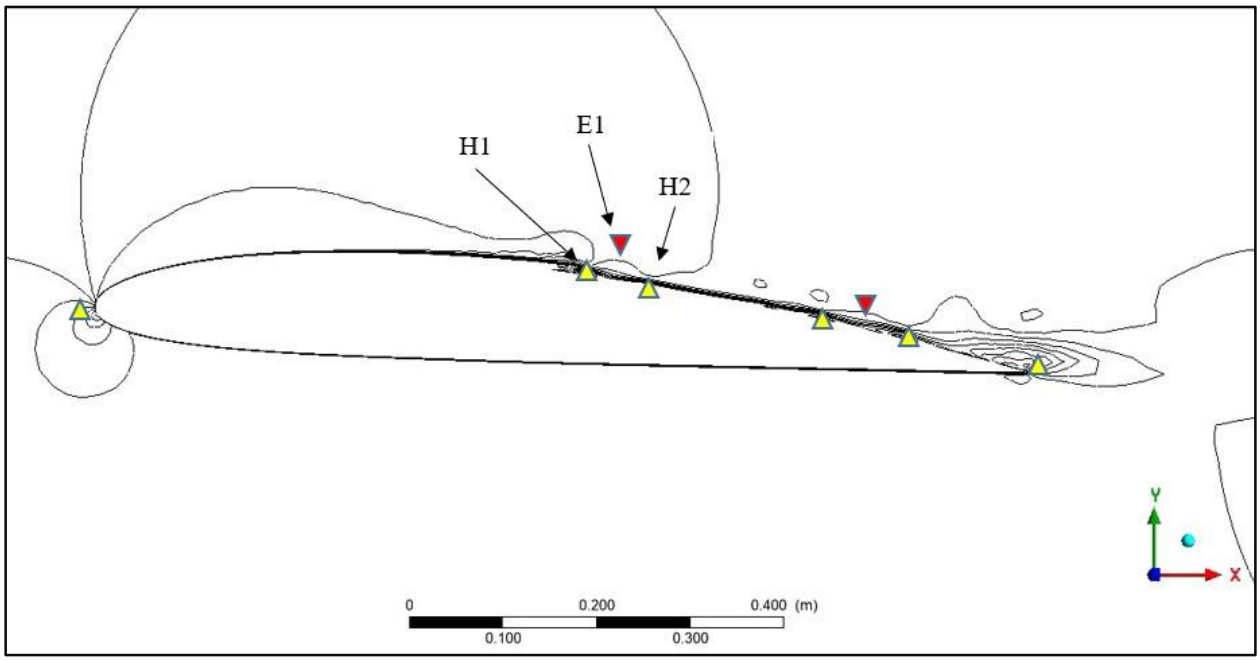

Fig. 15 - Flow topology around NACA 2411 at t_4 and $\alpha = 4^o$

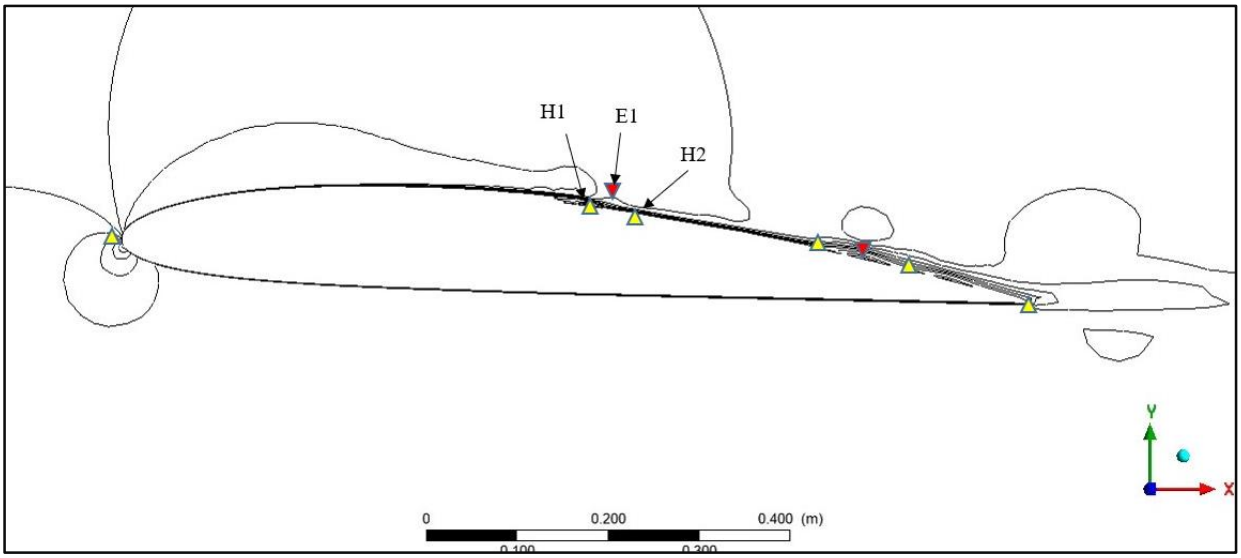

Fig. 16 - Flow topology around NACA 2411 at t_5 and $\alpha = 4^o$

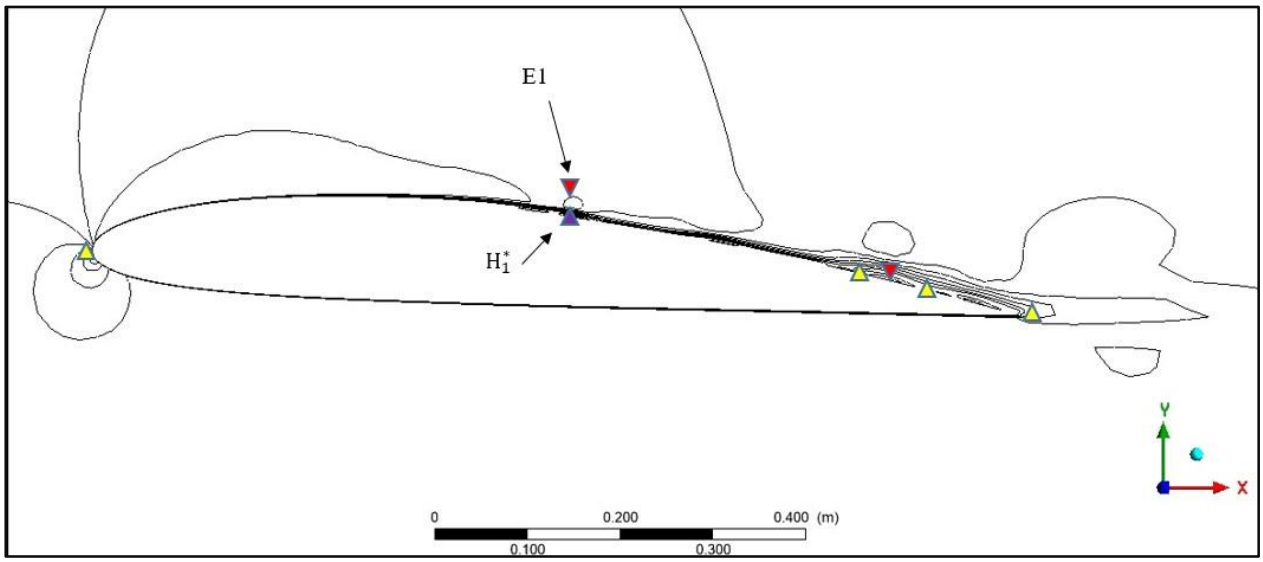

Fig. 17 - Flow topology around NACA 2411 at t_6 and α = 4°

3.3 NACA 0008

A hyperbolic fixed point was located on the leading edge of airfoil at t_1 as shown in Fig. 18. This moment was also the starting point for the formation of separation bubble. From t_2 to t_3 as in Fig. 19 and 20, a hyperbolic,H_1 and an elliptic,E_1 fixed points collided and cancelled each other in a reverse saddle node bifurcation. As can be seen clearly at t_3 in Fig. 20, H_1 and E_1 vanished.

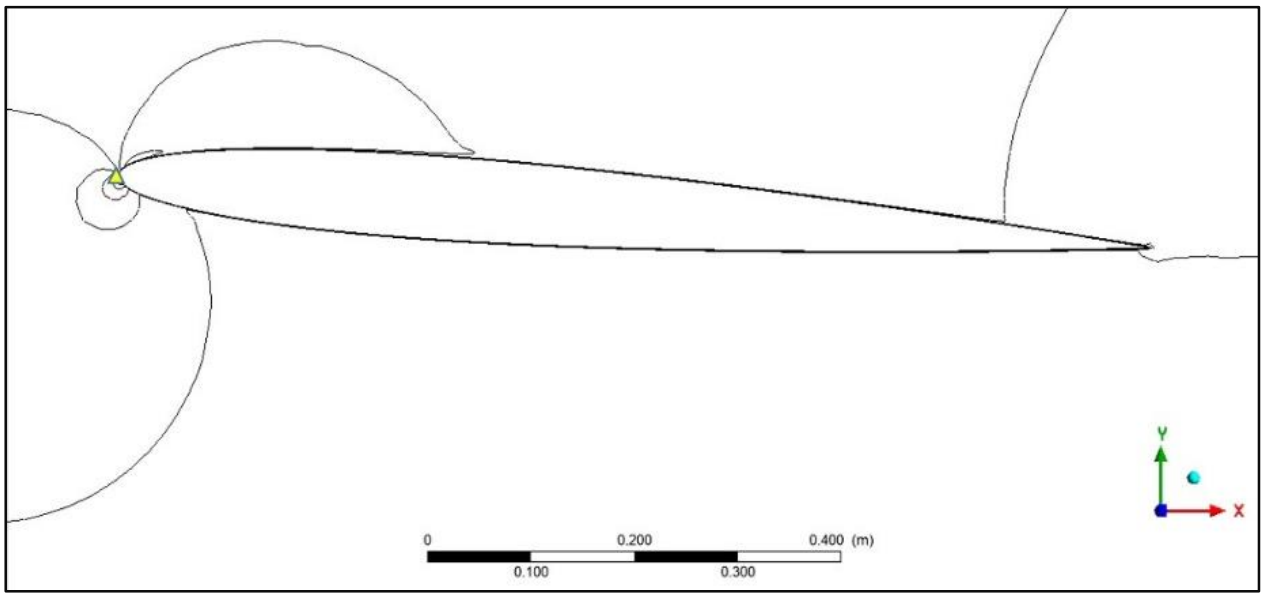

Fig. 18 - Flow topology around NACA 0008 at t_1 and α = 4°

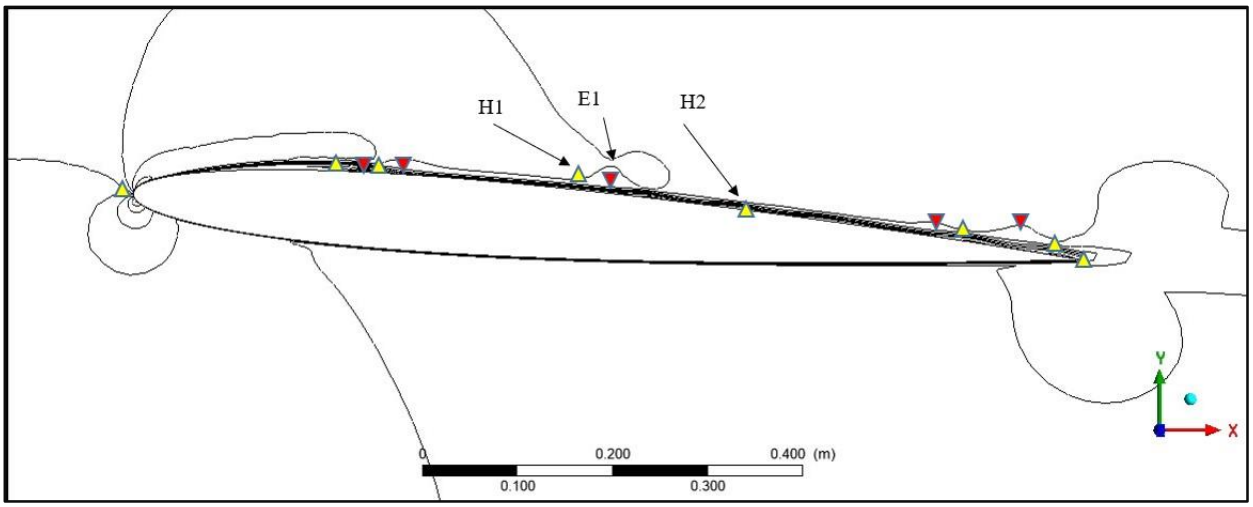

Fig. 19 - Flow topology around NACA 0008 at t_2 and α = 4°

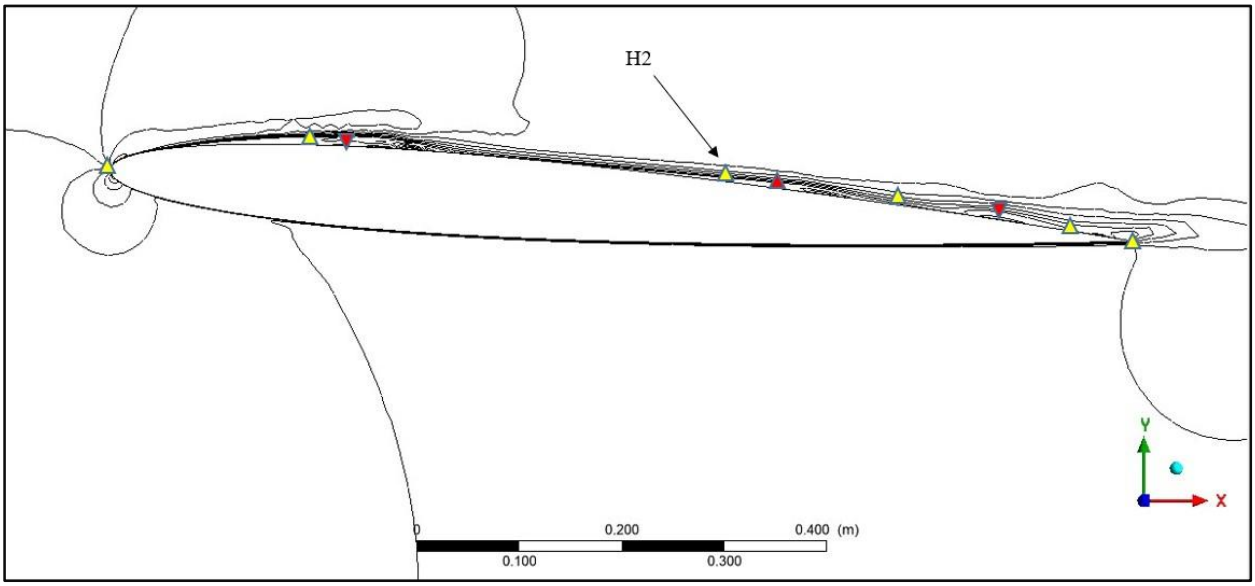

Fig. 20 - Flow topology around NACA 0008 at t_3 and α = 4°

From t_3 to t_6 as in Fig. 20 to Fig. 23, there was no collision of fixed points. However, there was a movement of separation bubble towards the trailing edge. Hyperbolic fixed points H_3 and H_4 collided in between t_5 and t_6 and separated from the airfoil's surface. It was hypothesized that the collision created a new hyperbolic point just below the shed vortex.

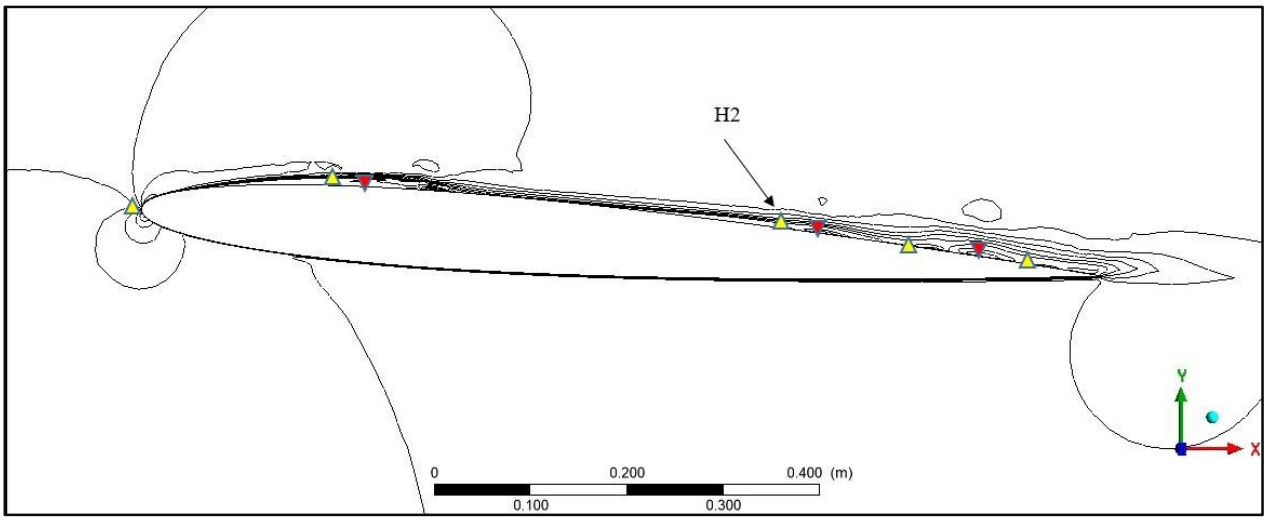

Fig. 21 - Flow topology around NACA 0008 at t_4 and $\alpha = 4^o$

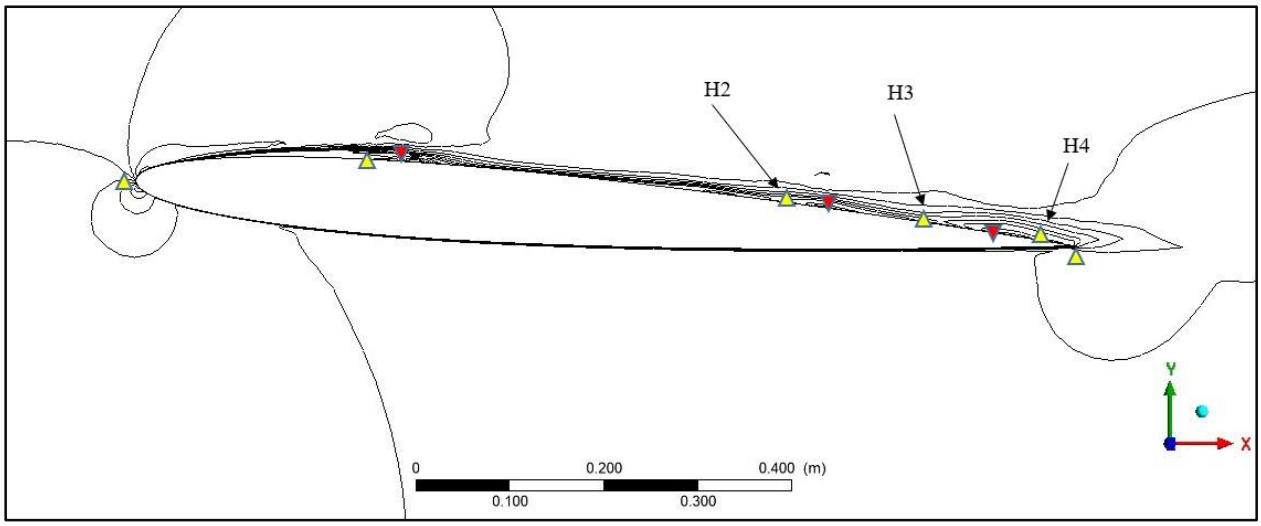

Fig. 22 - Flow topology around NACA 0008 at t_5 and $\alpha = 4^o$

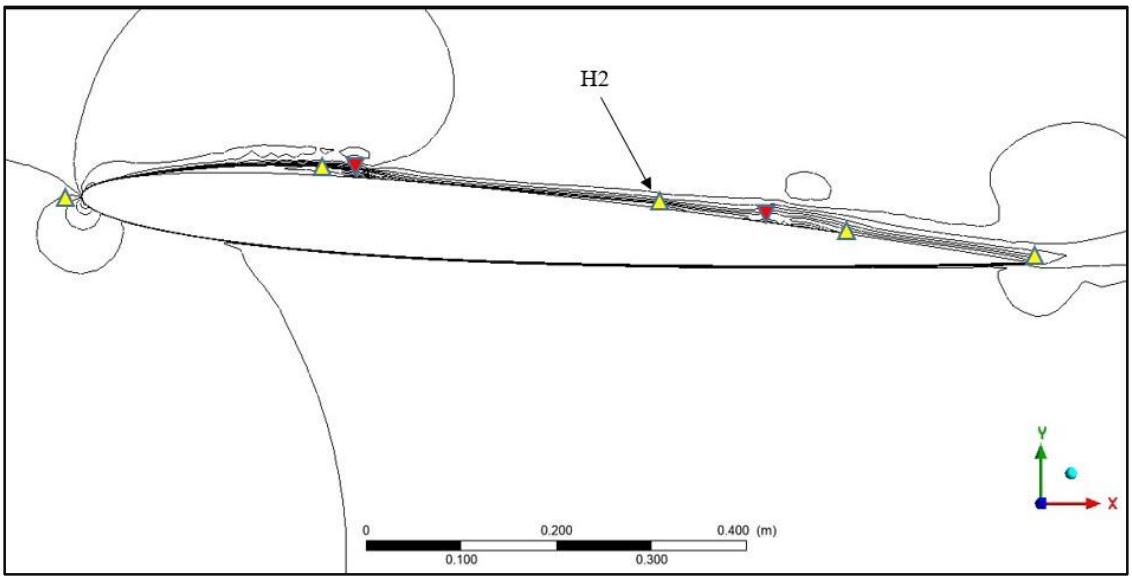

Fig. 23 - Flow topology around NACA 0008 at t_6 and $\alpha = 4^o$

3.4 Eppler 169

At t_1 as in Fig. 24, no significant fixed point was seen on the surface of the airfoil. At t_2, separation bubble was formed on the trailing edge. There were many hyperbolic and elliptic fixed points appeared at this time as shown in Fig. 25, including hyperbolic fixed points H_1 - H_8, and elliptic fixed points E_1 - E_4. It was obvious that the separation bubble moved to the middle of the airfoil surface and the vortices became bigger from t_2 to t_3 as in Fig. 25 and Fig. 26, respectively. Moreover, a new elliptic fixed point E_5 could later be observed at t_3 in Fig. 26 as the separation bubble increased in size.

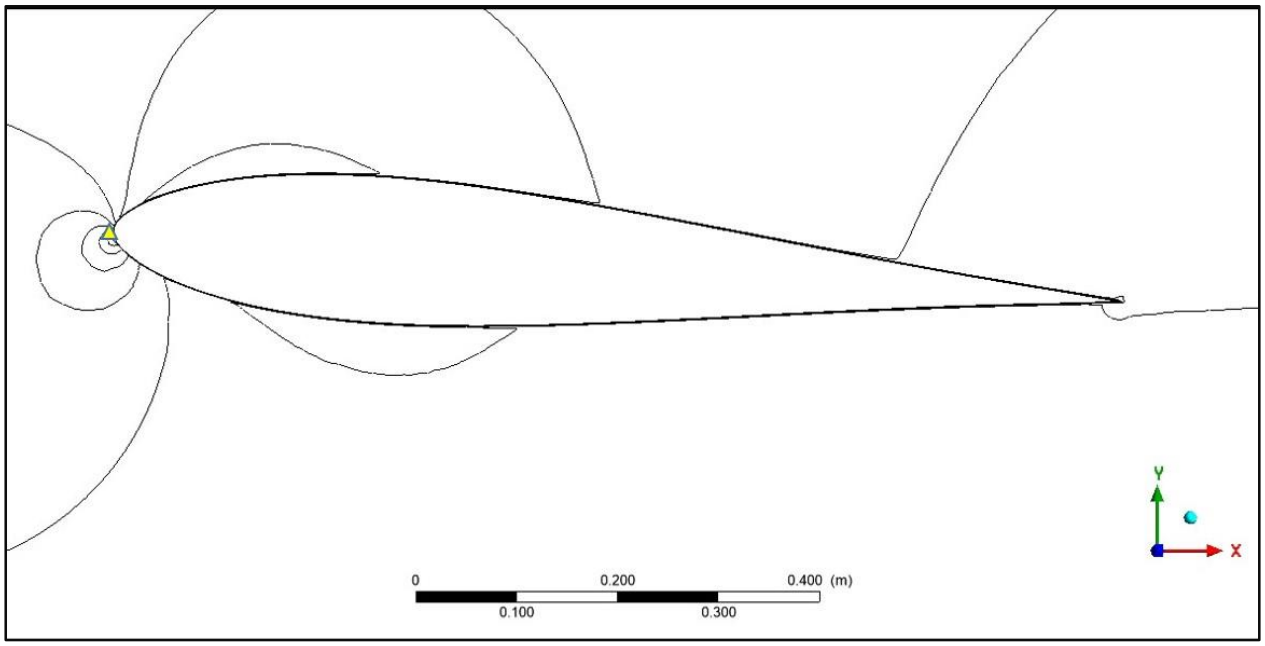

Fig. 24 - Flow topology around Eppler 169 at t_1 and $\alpha = 4°$

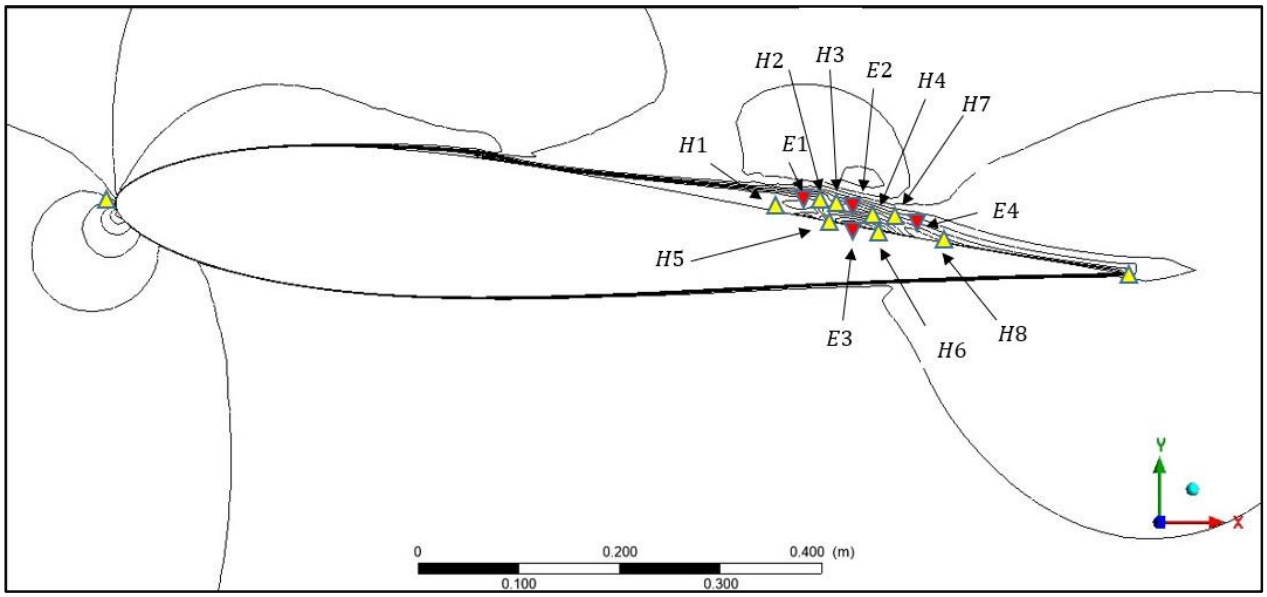

Fig. 25 - Flow topology around Eppler 169 at t_2 and $\alpha = 4°$

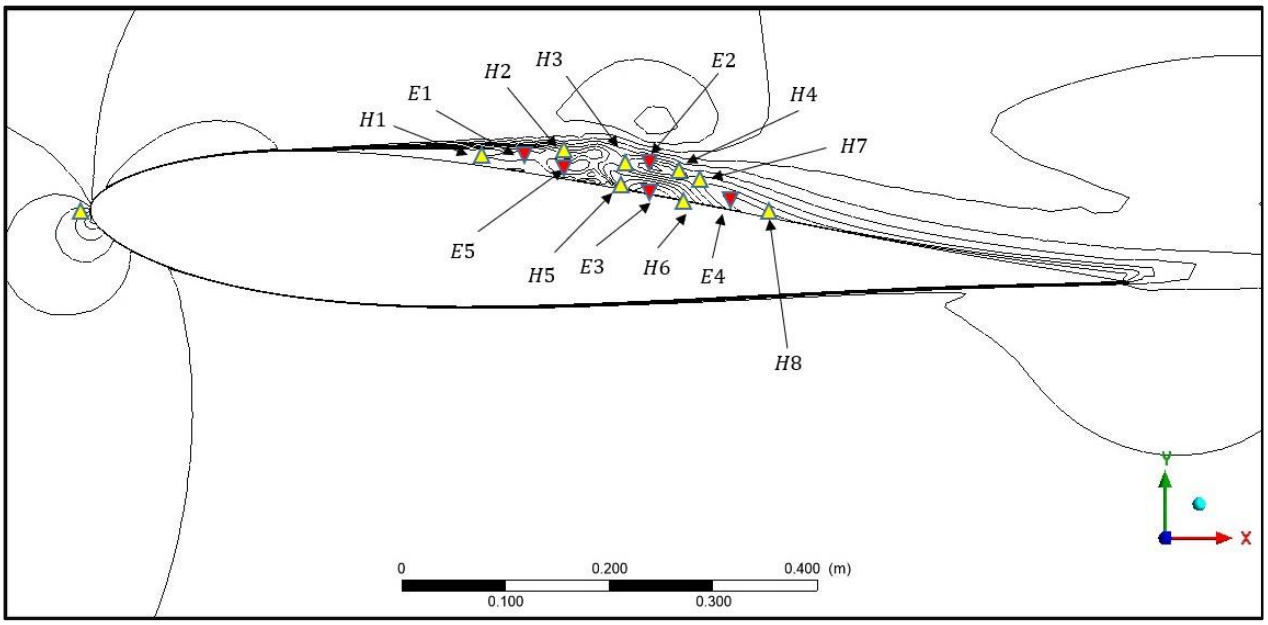

Fig. 26 - Flow topology around Eppler 169 at t_3 and $\alpha = 4^o$

At t_4 as in Fig. 27, it was seen that the separation bubble was drastically bigger in comparison to its size at t_3, and the reattachment point no longer presented since the flow was fully separated. Due to the separation bubble's size increment, the fixed points of hyperbolic and elliptic could now be more clearly seen. Hyperbolic fixed points H_7 and H_8 collided in between t_4 and t_5 in Fig. 28 and separated from the airfoil's surface. It was hypothesized that the collision created a new hyperbolic point just below the separated vortex prior to vortex shedding.

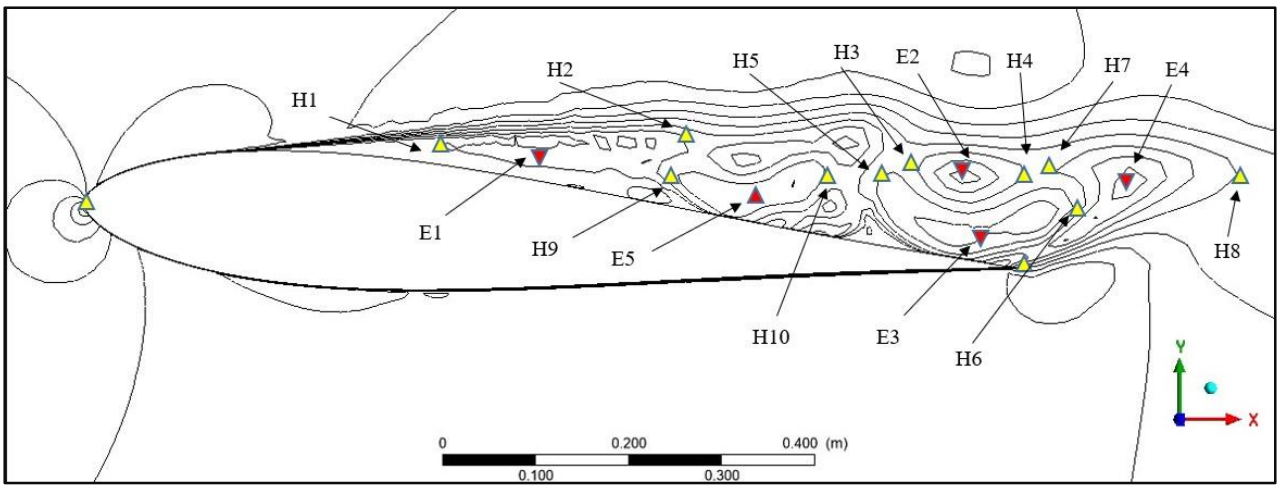

Fig. 27 - Flow topology around Eppler 169 at t_4 and $\alpha = 4^o$

There were two collisions at the transition from t_5 to t_6 in Fig. 28 and Fig. 29, respectively, involving hyperbolic fixed point H_9 with elliptic fixed point E_1, as well as hyperbolic fixed point H_2 with elliptic fixed point E_5. Consequently, a new elliptic fixed point E_{11} was formed.

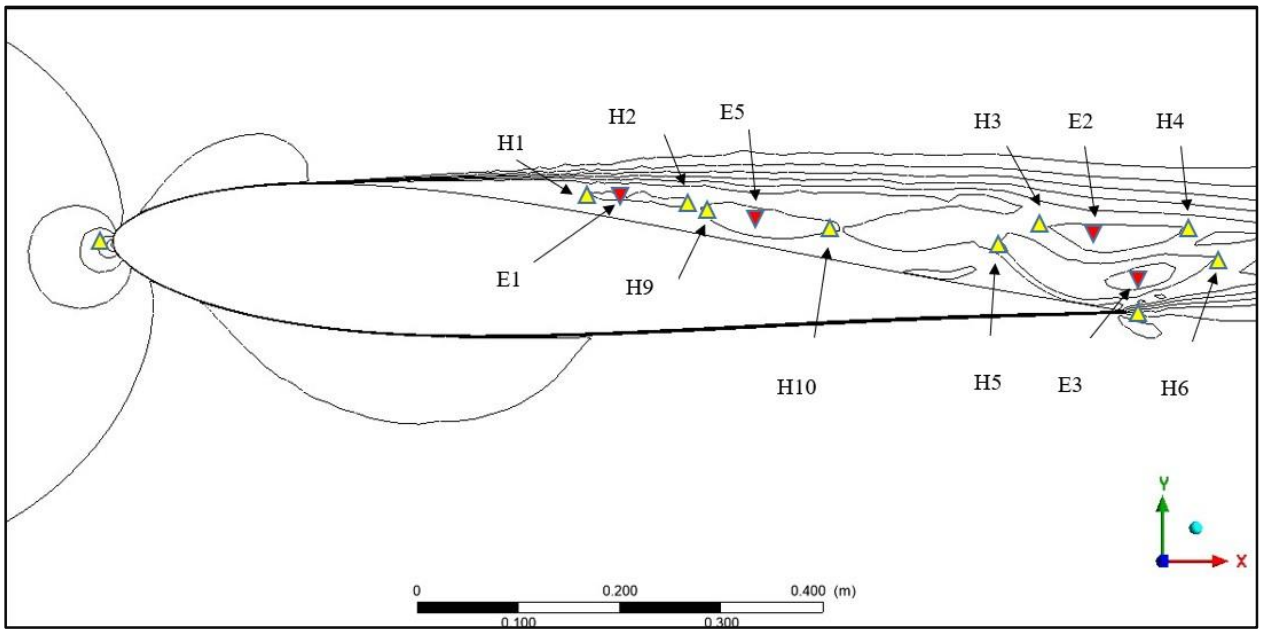

Fig. 28 - Flow topology around Eppler 169 at t_5 and $\alpha = 4°$

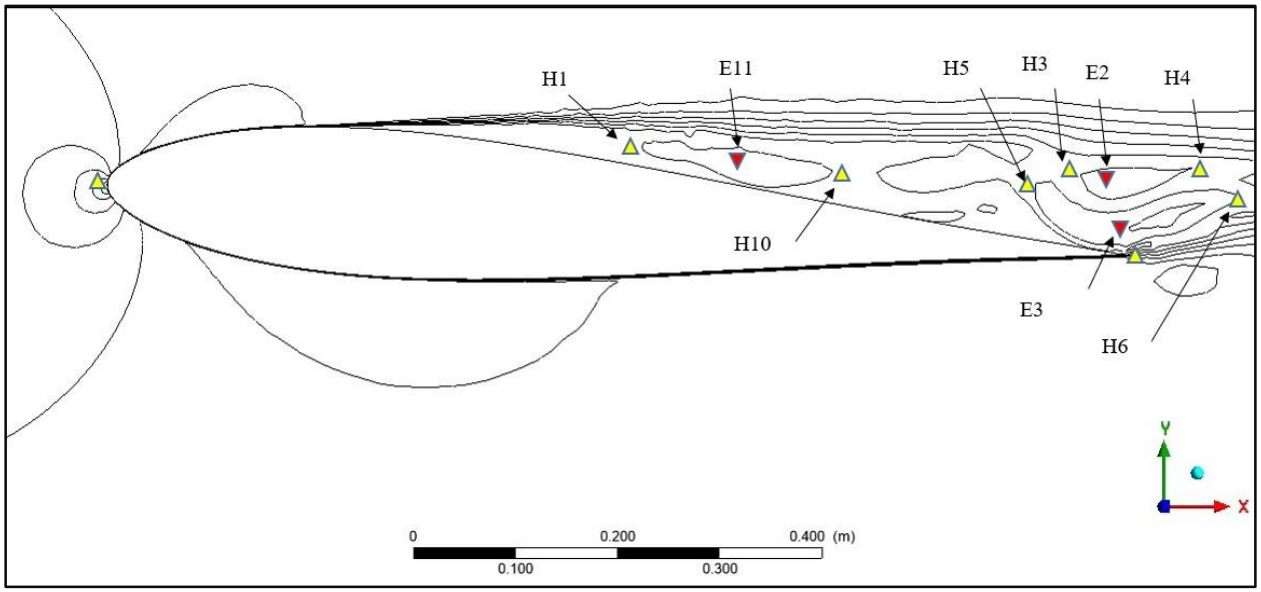

Fig. 29 - Flow topology around Eppler 169 at t_6 and $\alpha = 4°$

4. Conclusion

Most of the time, we could hypothesize the vortex shedding as in the case of Eppler 61, NACA 0008, and Eppler 169. It was physically spotted, however, in the case of NACA 2411. On the other hand, the separation bubble was easily identified in all cases. Furthermore, the flow topology around Eppler 169 airfoil highlighted the separation bubble which significantly changed in size with time, and the break of reattachment point due to full flow separation. Thus, flow topologies were clearly identified, and the comparative study was successfully implemented.

Acknowledgement

The authors would like to thank Faculty of Mechanical and Manufacturing Engineering, Universiti Tun Hussein Onn Malaysia for giving the opportunity to conduct this study.

References

Wang, L., & Peters, N. (2013). A new view of flow topology and conditional statistics in turbulence. *Philosophical Transactions of the Royal Society A: Mathematical, Physical and Engineering Sciences*, *371(1982)*, pp. 1-18.

Lipinski, D., Cardwell, B., & Mohseni, K. (2008). A Lagrangian analysis of a two- dimensional airfoil with vortex shedding. *Journal of Physics A: Mathematical and Theoretical, 41(34)*, pp. 1-22.

Bimbato, A. M., Alcântara Pereira, L. A., & Hirata, M. H. (2011). Study of the vortex shedding flow around a body near a moving ground. *Journal of Wind Engineering and Industrial Aerodynamics, 99(1),* pp. 7–17.

Kamemoto, K. (2004). On contribution of advanced vortex element methods toward virtual reality of unsteady vortical flows in the new generation of CFD. *Journal of the Brazilian Society of Mechanical Sciences and Engineering, 26,* pp. 368-378.

Ibrahim, C. I. H. C., & Abdullah, A. (2020). Flow topology around low Reynolds number airfoils with vortex shedding. *CFD Letters, 12(12),* pp. 85–103.

Hadi, M. I., Nazri, M., & Abdullah, A. (2006). Study of vortex behavior in unsteady flow over NACA 0012 and NACA 0024 airfoils. *ARPN J. Eng. Appl. Sci, 14,* pp. 3840-3846.

Faisal, A. F. A., Abdullah, A., Mohd, S., Rahim, M. Z., & Basuno, B. (2019). Classifying NACA airfoils based on thin airfoil theory. *ARPN J. Eng. Appl. Sci, 14(11),* pp. 2087-2093.

Grasso, F. (2013). Development of thick airfoils for wind turbines. *Journal of Aircraft, 50(3),* pp. 975–981.

Grasso, F. (2014). Modelling and effects of base drag on thick airfoils design. In *32nd ASME Wind Energy Symposium*, AIAA 2014-0168, pp. 1-9.

Shah, M. Z. M., Basuno, B., & Abdullah, A. (2020). Comparative study on several type of turbulence model available in ANSYS-Fluent software for ONERA M6 wing aerodynamic analysis. *Journal of Advanced Mechanical Engineering Applications, 1(1),* pp. 9-19.

Ahmed, M. R., Narayan, S., Zullah, M. A., & Lee, Y.-H. (2011). Experimental and numerical studies on a low Reynolds number airfoil for wind turbine blades. *Journal of Fluid Science and Technology, 6(3),* pp. 357–371.

Muiruri, P. I., & Motsamai, O. S. (2018). Three dimensional CFD simulations of a wind turbine blade section; validation. *Journal of Engineering Science and Technology Review, 11(1),* pp. 138–145.